Heliyon 10 (2024) e30444

Contents lists available at ScienceDirect

Heliyon

journal homepage: www.cell.com/heliyon

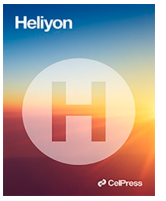

Research article

Augmented antitumor immune responses of HER2-targeted pyroptotic induction by long-lasting recombinant immunopyroptotins

Yuqi Xing [a], Feiyu Zhang [c], Tian Yang [d], Chunhui Yin [a], Angang Yang [b,**], Bo Yan [a,***], Jing Zhao [a,*]

[a] State Key Laboratory of Holistic Integrative Management of Gastrointestinal Cancers and Department of Biochemistry and Molecular Biology, Fourth Military Medical University, Xi'an, 710032, China
[b] State Key Laboratory of Holistic Integrative Management of Gastrointestinal Cancers and Department of Immunology, Fourth Military Medical University, Xi'an, 710032, China
[c] Department of Cardiology, Xijing Hospital, Fourth Military Medical University, Xi'an, 710032, China
[d] Department of Intensive Care Medicine, Bethune International Peace Hospital, Hebei, 050082, China

ARTICLE INFO

Keywords:
Pyroptosis
HER2
Immunopyroptotins
Targeted tumor therapy
Antitumor immunity

ABSTRACT

Pyroptosis is a well-documented form of programmed cell death caused by the gasdermin-driven perforation of cell membranes. Selective induction of pyroptosis in tumor cells represents a promising antitumor strategy to enhance the efficacy of immunotherapy. In this study, we established a recombinant protein-based immunopyroptotin strategy that led to the intratumoral induction of pyroptosis for HER2-directed therapy. Long-lasting immunopyroptotins were constructed by sequentially fusing the humanized anti-HER2 single-chain antibody P1h3, albumin-binding peptide (ABD035 or dAb7h8), cathepsin B-cleavable peptide B2, endosome-disruptive peptide E5C3, and active pyroptotic effector gasdermin D-N fragment (GN). After purification, we evaluated the cytotoxicity and antitumor immune responses primarily induced by the immunopyroptotins in HER2-overexpressing breast cancer cells. The resulting ABD035-immunoGN and dAb7h8-immunoGN showed improved in vitro cytotoxicity in HER2-overexpressing cancer cells compared with that in the immunotBid that we previously generated to induce tumor cell apoptosis. The binding of long-lasting immunopyroptotins to albumin increased the half-life by approximately 7-fold in nude mice. The enhanced antitumor efficacy of long-lasting immunopyroptotins was confirmed in both N87 tumor-bearing T cell-deficient mice and 4T1-hHER2 bilateral tumor-bearing immunocompetent mice. Immunopyroptotin treatment elicited systemic antitumor immune responses involving $CD8^+$ T cells and mature dendritic cells and upregulated the expression of proinflammatory cytokines, leading to sustained remission of non-injected distant tumors. This study extends the repertoire of antibody-based therapeutics

* Corresponding author. State Key Laboratory of Holistic Integrative Management of Gastrointestinal Cancers and Department of Biochemistry and Molecular Biology, Fourth Military Medical University, Xi'an, No. 169 Changle West Road, Shaanxi 710032, China
** Corresponding author. State Key Laboratory of Holistic Integrative Management of Gastrointestinal Cancers and Department of Immunology, Fourth Military Medical University, Xi'an, No. 169 Changle West Road, Shaanxi 710032, China
*** Corresponding author. State Key Laboratory of Holistic Integrative Management of Gastrointestinal Cancers and Department of Biochemistry and Molecular Biology, Fourth Military Medical University, Xi'an, No. 169 Changle West Road, Shaanxi 710032, China
E-mail addresses: agyang@fmmu.edu.cn (A. Yang), yb5870@163.com (B. Yan), zhaojing@fmmu.edu.cn (J. Zhao).

https://doi.org/10.1016/j.heliyon.2024.e30444
Received 2 December 2023; Received in revised form 25 April 2024; Accepted 26 April 2024
Available online 27 April 2024

through the tumor-targeted delivery of a constitutively active pore-forming gasdermin-N fragment, which shows great potential for pyroptosis-based antitumor therapy.

1. Introduction

HER2 is overexpressed in various carcinomas and recognized as a target for antitumor therapy. Substantial progress has been made on HER2-targeted therapies since the development of anti-HER2 antibodies and their derivatives [1,2]. Monoclonal antibodies against HER2, including trastuzumab and pertuzumab, and antibody-drug conjugates, such as T-DM1, have been used clinically. However, these drugs have shown limited efficacy, drug resistance, and cardiotoxicity when used as single-drug treatment [3–6]. In addition, clinical trials are ongoing for HER2-directed immunotoxins, which comprise a single-chain antibody (scFv) and toxins sourced from plants and bacteria. However, safety concerns persist regarding the production of neutralizing antibodies and liver toxicity [7–10]. Other immunoconjugated proteins, including cytokines, nucleases, and pro-apoptotic effectors, are currently under preclinical investigation. Among these, a series of immunoapoptotins that can bypass HER2 downstream signaling have been generated, thus directly inducing tumor cell apoptosis. This immunoapoptotic strategy can effectively kill trastuzumab-resistant HER2 positive tumor cells [11–16]. ImmunotBid emerged as the top performer in our previous reports [16], but it requires further modification to facilitate faster initiation of cell death and a longer half-life in serum. Therefore, in this study, we used immunotBid as the parental formula for structural modifications (see Scheme 1).

Our first attempt was to improve the cell death-inducing strategy by transforming the mode of tumor cell death from apoptosis to pyroptosis. Pyroptosis is a natural defence mechanism of the innate immune system. This mode of cell death occurs between apoptosis and necrosis. Pyroptotic cells appear as bubble-like bulges on the cell membrane surface, swelling, and cellular lysis, leading to the release of proinflammatory factors [17–20]. The kinetics of pyroptosis are faster than those of apoptosis. Upon cleavage, members of the pyroptosis effector gasdermin (GSDM) family release their N-terminal domain, which can directly form pores in the cell membrane, leading to rapid cell death [17–19,21]. Importantly, either overexpression of the N-terminal domain gene fragment of GSDMD (GN) or

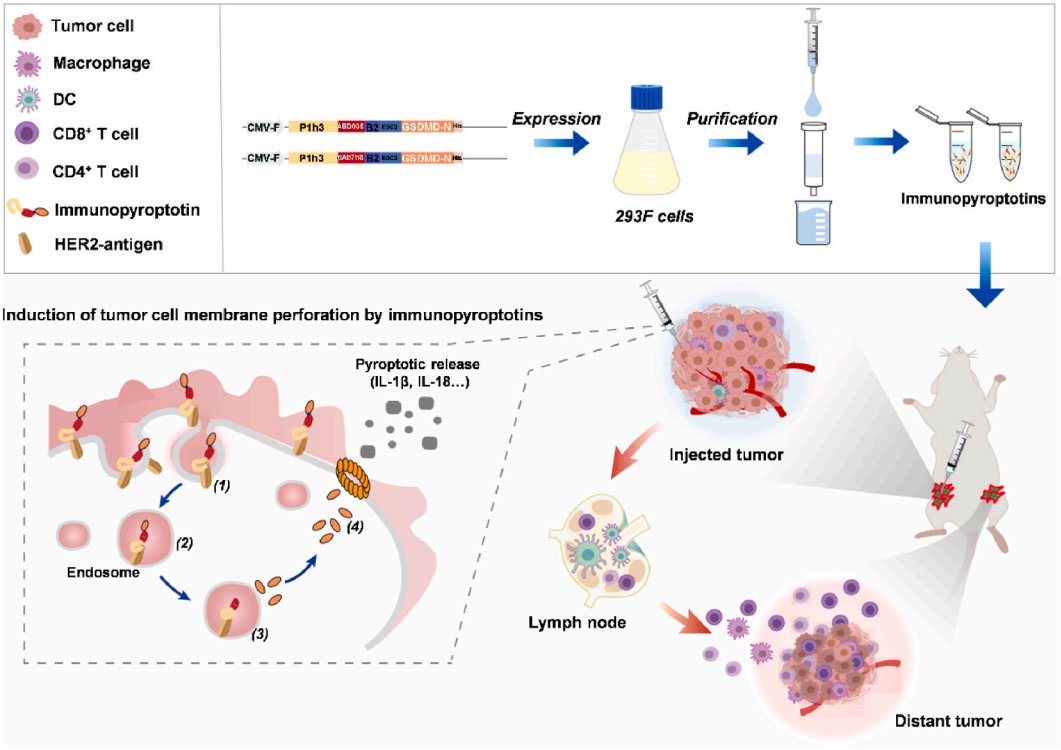

Scheme 1. Schematic illustration of the use of immunopyroptotins for antitumor therapy by HER2-targeted induction of pyroptosis. The immunopyroptotins consist of the humanized anti-HER2 single-chain antibody P1h3, albumin-binding peptide (ABD035 or dAb7h8), cathepsin B-cleavable peptide B2, endosome-disruptive peptide E5C3, and active pyroptotic effector gasdermin D-N fragment (GSDMD-N). The fusion proteins are expressed in 293F cells and purified using Ni^{2+}-NTA affinity chromatography. The immunopyroptotins are then injected into a unilateral tumor in immunocompetent mice with bilateral xenograft breast tumors. Upon recognition and subsequent endocytosis into HER2-positive tumor cells, the immunopyroptotins are cleaved at the B2 site by cathepsin B in the endosomes, and GSDMD-N is released into the cytosol via E5C3-mediated endosomal escape, finally inducing tumor cell pyroptosis. Systemic immune responses are elicited by the accumulation of $CD8^+$ T cells, mature DCs, and upregulated expression of proinflammatory cytokines, leading to sustained remission of the distant tumor as well as the injected tumor.

cellular introduction of the GN protein would be sufficient to induce pyroptosis [18,19,21]. Therefore, the induction of pyroptosis in tumor cells is considered a feasible antitumor strategy. Based on our previous immunotBid formula, we aimed to enhance tumor-killing efficiency by substituting the proapoptotic tBid with the propyroptotic GN, resulting in the development of immunoGN.

Our second attempt was to prolong half-life by structurally inserting an albumin-binding moiety. We introduced an albumin-binding domain into immunoGN between scFv and the translocation moiety. The modified immunoGN is designed to interact with albumin, evading lysosomal degradation through protective binding to the FcRn receptor [22]. This interaction leads to an extended serum lifetime for the immunoGN-albumin complex. In the present study, two types of albumin-binding peptides, the streptococcal protein G derivative ABD035 [23–25] and the human anti-albumin single-domain antibody dAb7h8 [26–28], were tested for their ability to confer long-lasting activity to the resultant ABD035-immunoGN and dAb7h8-immunoGN constructs.

Herein, we constructed a novel class of long-lasting immunopyroptins by sequentially fusing humanized anti-HER2 scFv P1h3 [16], albumin-binding peptides (ABD035 or dAb7h8), cathepsin B-cleavable peptide B2 [29–31], endosome-disruptive peptide E5C3 [32], and propyroptotic GN. In theory, albumin-bound immunoGN recognizes HER2-positive tumor cells, enters endosomes, and is cleaved to release GN, thereby inducing pyroptosis. The putatively enhanced tumor-killing and long-lasting effects were evaluated in vitro and in vivo and compared with those of the parental immunotBid molecule.

2. Materials and methods

2.1. Construction, expression, and purification

The genes encoding P1h3-ABD035-B2-E5C3-GN-His (abbreviated as ABD035-immunoGN), P1h3-dAb7h8-B2-E5C3-GN-His (dAb7h8-immunoGN), P1h3-B2-E5C3-GN-His (immunoGN), and P1h3-B2-E5C3-tBid-His (immunotBid) were inserted into the eukaryotic expression vector pcDNA3.1 using the restriction enzymes *Bam*HI and *Eco*RI. The resulting recombinant plasmids were verified through DNA sequencing.

The recombinant plasmids were transfected into 293F cells. After 5 d, the cells were harvested and sonicated for 2 min on ice. The expression of the fusion proteins was determined using Western blot and sodium dodecyl sulfate-polyacrylamide gel electrophoresis (SDS-PAGE).

For protein purification, the cell precipitates were purified using Ni^{2+}-NTA buffer without imidazole. We used Ni^{2+}-NTA His Bind Resins (Novagen, Madison, WI, USA) for Ni^{2+}-NTA affinity chromatography according to the manufacturer's instructions. The bound proteins were eluted with 10 mM imidazole buffer at 25 °C, and then analyzed using SDS-PAGE and quantified using the bicinchoninic acid (BCA) assay (Thermo Fisher Scientific, Waltham, MA, USA).

2.2. Cell culture

Human embryonic kidney FreeStyle 293F (CVCL_D603; catalogue number: PTA-5080), SKBR-3 breast cancer (CVCL_0033; catalogue number: HTB-30; human mammary adenocarcinoma cells with high expression of HER2), N87 gastric carcinoma (CVCL_1603; catalogue number: CRL-5822; human gastric tubular adenocarcinoma cells with high expression of HER2), NCI–H1975 (CVCL_1511; catalogue number: CRL-5908; human lung adenocarcinoma cells with modest expression of HER2), and 4T1 murine breast cancer cells (CVCL_0125; catalogue number: CRL-2539; murine mammary carcinoma cells) were obtained from American Type Culture Collection (Manassas, VA), and then transduced with human HER2 gene to generate 4T1-hHER2 cells. PC9 lung adenocarcinoma cell lines (CVCL_B260; catalogue number: 305045; human lung adenocarcinoma cells without HER2 expression) were purchased from CLS Cell Lines Service GmbH (Eppelheim, Germany); of them, 293F cells were cultured in FreeStyle 293F expression medium (Gibco, Waltham, MA, USA), and SKBR-3 cells were grown in McCoy's 5A medium supplemented with 10 % (v/v) fetal bovine serum (FBS) (Sigma-Aldrich, Merck KGaA, Germany) and 1 % (v/v) penicillin–streptomycin (Hyclone, Logan, UT). N87, NCI–H1975, and PC9 cells were cultured in RPMI-1640 medium supplemented with 10 % (v/v) FBS (Sigma-Aldrich, Merck KGaA, Germany) and 1 % (v/v) penicillin–streptomycin (Hyclone, Logan, UT). All cells were incubated at 37 °C in a 5 % CO_2 incubator.

2.3. Purified protein identification via SDS-PAGE and western blotting

Proteins were analyzed using SDS-PAGE. Samples were electrophoresed at 80 V for 20 min in a 5 % concentrating gel and then at 120 V in a 10 % separating gel until bromophenol blue reached the bottom of the gel plate. The gel was stained with Coomassie Brilliant Blue R250 (Sigma-Aldrich, Merck KGaA, Germany) for 30–60 min and decolorized overnight until the background became transparent. The purity of the expressed proteins was assessed through grayscale analysis of the electrophoresis gel using ImageJ Software (ImageJ, Maryland, USA). Immunoblotting using nitrocellulose membranes (NC membranes) (Millipore, Bedford, MA, USA) was performed to identify the proteins of interest. After blocking with 3 % bovine serum albumin (BSA, V900933, Sigma-Aldrich) for 1 h at 25 °C, the membranes were incubated with mouse anti-His antibody (2366T, 1:1000, Cell Signaling Technology, Danvers, MA, USA), rabbit anti-GSDMD-N (ab215203, 1:1000, Abcam, MA, USA), and rabbit anti-GAPDH (5174T, 1:1000, Cell Signaling Technology, Danvers, MA, USA) at 4 °C overnight. After washing three times for 30 min, the membranes were incubated with IRDye 800CW goat anti-mouse secondary antibody (926–32210, 1:20000, LI-COR Biosciences, Lincoln, USA) and goat anti-rabbit secondary antibody (7074P2, 1:3000, Cell Signaling Technology, Danvers, MA, USA) for 1 h at 25 °C. The membrane was visualized employing the Odyssey infrared imaging system (LI-COR Biosciences, Lincoln, USA) and ECL Prime Western Blotting Detection Reagent (GE Healthcare, USA).

2.4. Albumin-binding assay

Human serum albumin (HSA, 1 μg/mL, A1653, Sigma-Aldrich) or murine serum albumin (MSA, 1 μg/mL, A3139, Sigma-Aldrich) in 1 × phosphate-buffered saline (PBS) was coated in 96-well enzyme-linked immunosorbent assay (ELISA) plates at 4 °C overnight. ABD035-immunoGN, dAb7h8-immunoGN, and immunoGN (1 mg/mL) were added and incubated for 2 h at 25 °C, followed by incubation with the anti-His antibody at 25 °C for 2 h. After being extensively washed six times with wash buffer (0.05 % Tween 20 in 1 × PBS), a secondary horseradish peroxidase (HRP)-conjugated antibody was added and detected using TMB substrate (Thermo Fisher Scientific, Waltham, MA, USA). Data were analyzed using GraphPad Prism software (version 8.0; GraphPad Software Inc., USA).

2.5. Cytotoxicity assay of cell pyroptosis

After seeding 1×10^4 SKBR-3 cells into 96- and 1×10^5 SKBR-3 cells into 12-well plates, the cells were incubated with 1 mg/mL immunopyroptotins for the indicated times. After washing with 1 × PBS, the cells in the 96-well plates were treated with ABD035-immunoGN, dAb7h8-immunoGN, and immunotBid for 12 and 24 h. Supernatants in the 96-cell plates were collected for lactate dehydrogenase (LDH) measurements (Promega, Madison, WI, USA), while cells were treated with 10 μL CCK-8 solution (Promega, Madison, WI, USA); the absorbance was measured at 450 nm using a microplate reader (BioTek, Winooski, VT, USA) to calculate cell viability. Supernatants and cells in 12-well plates were treated with the indicated proteins for 24 h. After washing twice with 1 × PBS, samples (5×10^5 cells) were analyzed using a BD FACS Aria III flow cytometer (BD Biosciences, Franklin Lakes, NJ, USA). The obtained data were analyzed using FlowJo software. The pyroptotic morphology was observed using an optical microscope (Olympus IX71, Tokyo, Japan). The blood plasma and tumor tissues were collected from ABD035-immunoGN-treated Balb/c mice, and the levels of IL-1β (MLB00C, R&D Systems, MN, USA), IL-18 (7625, R&D Systems, MN, USA), and HMBG1 (NBP2-62767, Novus, CO, USA) were detected via ELISA according to the manufacturer's guidance.

2.6. Animal housing and tumor inoculation

Female nude mice (6–8 weeks old, weighing 20–25 g, n = 40) and female BALB/c mice (6–8 weeks old, weighing 20–25 g, n = 53) were purchased from the Fourth Military Medical University Laboratory Animal Center. Three to five mice were housed in each cage under pathogen-free conditions with a 12/12-h light/dark cycle and *ad libitum* access to food and water. All the experimental procedures were approved by the Animal Experimental Ethics Committee of the Fourth Military Medical University (Ref. No. IACUC-20200655).

The N87 xenograft mouse model was established by the subcutaneous implantation of 5×10^6 N87 cancer cells into the right hind limbs of nude mice. Tumor growth was monitored by palpation every 5 d. A total of 1×10^6 4T1-hHER2 cells were injected into the mammary fat pads of BALB/c mice on the right side of the abdomen (injected tumor), and 5×10^5 4T1-hHER2 cells were injected into the left mammary fat pads (distant tumor) to establish a 4T1-hHER2 tumor-bearing mouse model. For 25 d, tumor growth was monitored by palpation every 5 d, and tumor volume was calculated using the following formula: volume = (length × width^2)/2.

2.7. Evaluation of in vivo half-life

To determine protein half-life in blood circulation, four groups of five female BALB/c mice each were injected intravenously with 0.1 μmol/kg of the indicated proteins. Blood samples were promptly collected at 5, 10, 30, 60, 360, and 720 min. The protein concentration was measured using a cell-based ELISA. Briefly, 96-well ELISA plates were seeded with 1×10^4 SKBR-3 cells for 24 h. After fixing with 4 % paraformaldehyde (PFA) and blocking with 2 % BSA, serum samples were added followed by incubation with an anti-His mouse antibody (2366T; Cell Signaling Technology) at 25 °C for 2 h. After extensive washing, an HRP-conjugated anti-mouse antibody (K0055G-HRP; Solarbio, Beijing, China) was added for 1 h and detected using TMB substrate (Thermo Fisher Scientific, Waltham, MA, USA). Based on the 5-min sample value, the data were analyzed using a "one-phase decay" model in GraphPad Prism.

2.8. In vivo tracing of the long-lasting immunopyroptotins

The long-lasting immunopyroptotins were labeled with DyLight 800 NHS Ester (Thermo Fisher Scientific, Waltham, MA, USA) according to the manufacturer's instruction. A Zeba spin-desalting column was used to remove the unreacted dye. After incubation, 4T1-hHER2 tumor-bearing BALB/c mice were injected intravenously with 0.1 μmol/kg of the labeled proteins for 10 min. The distribution of the proteins in major organs was detected through imaging using the IVIS® Lumina II in vivo imaging system (PerkinElmer, Thermo Fisher, MA, USA).

2.9. RNA isolation and quantitative real-time PCR

Total RNA was isolated from tumor tissues using the TRIzol reagent (Invitrogen, Waltham, MA, USA) according to the manufacturer's instructions. A PrimeScript First-Strand cDNA Synthesis Kit (Takara, Kusatsu, Japan) was used for reverse transcription, and quantitative real-time PCR was performed using SYBR Green qPCR Master Mix (Thermo Fisher Scientific, Waltham, MA, USA). Primers for *Il-10, Il-2, Ifn-γ, Foxp3, Tgf-β,* and *mouse β-actin* used in this study are listed in Supplementary Table S1. All reactions were performed at least in triplicate, and the target mRNA expression levels were normalized to those of *mouse β-actin.* The relative mRNA expression

was calculated using the $2^{-\Delta\Delta Ct}$ method [33].

2.10. Flow cytometry

Tumor tissue samples and lymph nodes were collected and dissociated into homogenates for 30 min using a Gentle MACS Dissociator with type I collagenase (Gibco, Waltham, MA, USA). Single-cell suspensions were washed with red cell lysis solution, filtered through 70 μm nylon mesh filters, and washed using 1 × PBS. To analyze active T cell infiltration into tumors and lymph nodes, single-cell suspensions were stained with PE-*anti*-CD3 (BioLegend, 100308) and APC-*anti*-CD8 (BioLegend, 100711). To analyze mature dendritic cells (DCs), single-cell suspensions were stained with APC-*anti*-MHC II (Biolegend, 116417) and FITC-*anti*-CD11c (Biolegend, 117305) according to the manufacturer's protocols. Data were analyzed using a Beckman CytoFLEX (Beckman Coulter, Brea, CA, USA) and FlowJo V10 software.

2.11. Immunofluorescent microscopy

After fixation in 4 % PFA, the tumor tissues and lymph nodes were dehydrated in a 20 % sucrose solution, embedded in paraffin, and subsequently cut into slices (5 μm). After incubation with 5 % BSA for 1 h, primary antibodies were added (anti-CD3, 1:500, GB13014; anti-CD4, 1:500, GB11064; anti-CD8, 1:2000, GB12068; anti-Foxp3, 1:500, GB13445; anti-CD68, 1:200, GB113109; anti-Ki67, 1:600, GB121141; anti-CD86, 1:300, GB13585; anti-CD11c, 1:300 GB11059, all from Servicebio, Wuhan, China) at 4 °C in a dark, wet box overnight. After extensive washing using FACS buffer, sections were incubated with secondary antibodies (FITC-goat anti-rat, 1:200, GB22302; CY3-goat anti-rabbit, 1:500, GB21301; Alexa Fluor 488-goat anti-mouse, 1:500, GB25301, all from Servicebio) for 1 h at 25 °C. Nuclei were stained with Hoechst 33342 (Thermo Fisher Scientific, Waltham, MA, USA). The stained sections were observed using a Nikon A1 spectral confocal microscope (Nikon, Tokyo, Japan).

2.12. Histological examination and TUNEL

Immediately after intraperitoneal anesthesia and euthanasia, the mice were perfused with saline and 4 % PFA. The heart, lung, liver, spleen, and kidney were extracted and fixed in 4 % PFA for 24 h, embedded into paraffin, and subsequently sectioned into 5 μm. Sections were stained with hematoxylin and eosin (Beyotime, Beijing, China) and observed using a Nikon A1 spectral confocal microscope (Nikon, Tokyo, Japan). Dead cells in major organ sections were stained using a TUNEL Apoptosis Detection Kit (Promega).

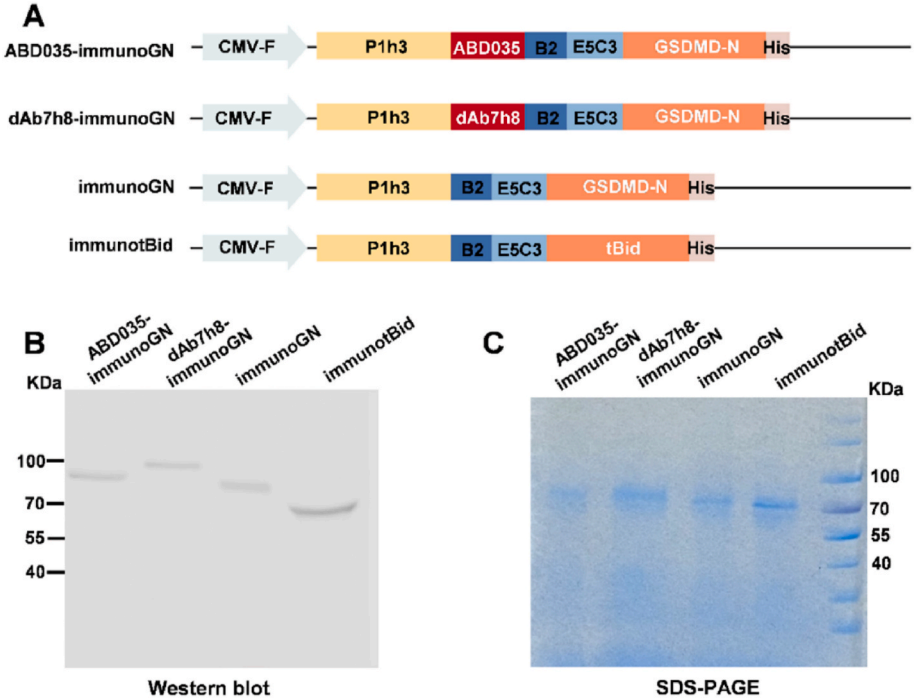

Fig. 1. Identification of purified long-lasting immunopyroptotins. (A) Schematic showing the construct of various immunopyroptotins and immunotBid used in this study. (B, C) Purification of proteins expressed in eukaryote systems identified using western blotting (B) and SDS-PAGE (C).

2.13. Lung metastasis

Thirty days after tumor cell inoculation, the lungs were collected from 4T1-hHER2 bilateral tumor-bearing BALB/c mice, washed with PBS, and fixed in Bouin's fixative. The nodules in the lungs were counted manually. Fixed lung tissues were stained with hematoxylin and eosin (Beyotime, Beijing, China) according to a previously described histological examination method.

2.14. Detection of liver function and renal function

Tumor-bearing mice were killed after the ABD035-immunoGN treatment, and the blood samples of the treated mice were collected for serum isolation through centrifugation of 4000 rpm for 15 min at 4 °C. Serum ALT (S03030; Rayto, Shenzhen, China), AST (S03040; Rayto, Shenzhen, China), and CREA (S03076; Rayto, Shenzhen, China) levels were determined according to the manufacturer's instructions.

2.15. Statistical analysis

All data are expressed as mean ± standard error of the mean (SEM) and were analyzed using *t*-test, two-way analysis of variance, and log-rank tests. Differences were considered statistically significant at $p < 0.05$. Statistical analyses were performed using GraphPad Prism software 8.0.

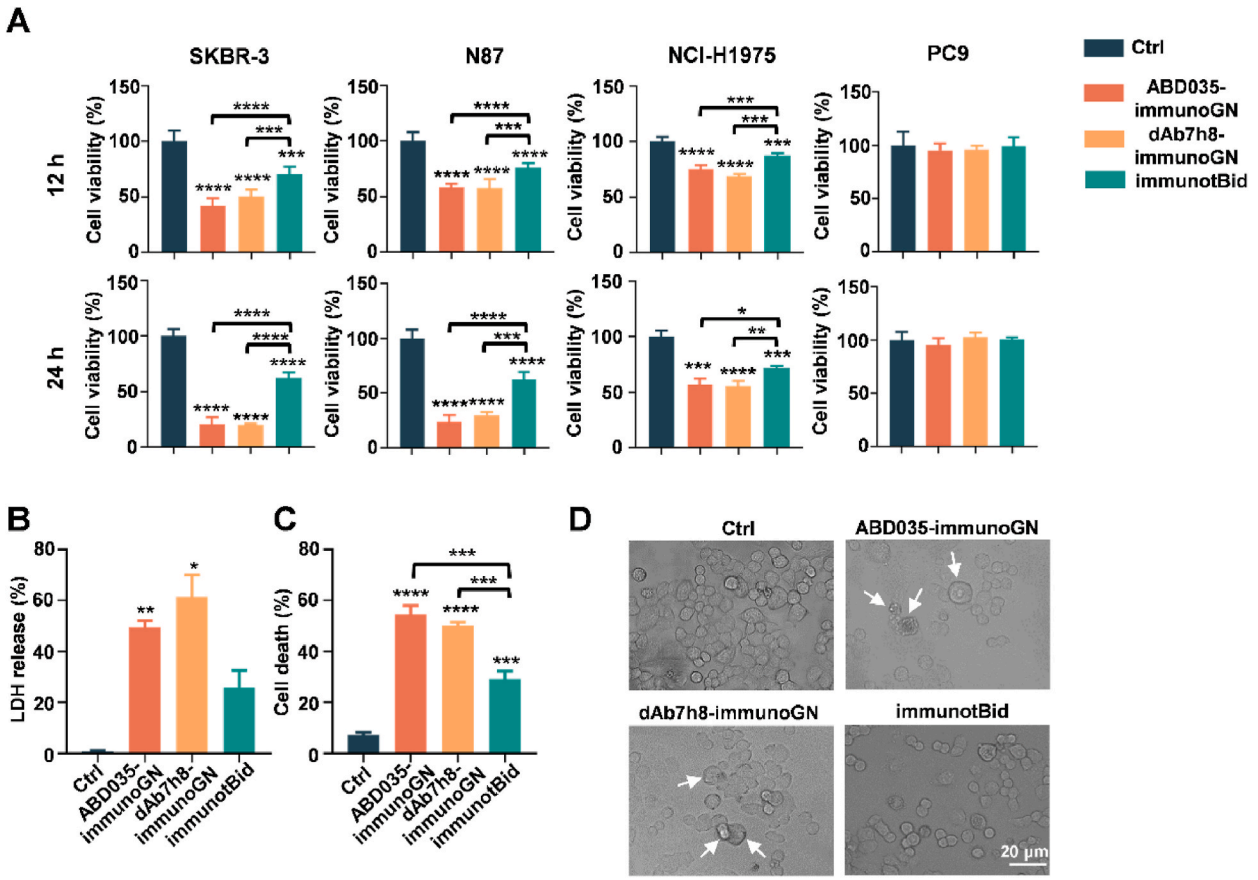

Fig. 2. Killing capacity of the long-lasting immunopyroptotins in vitro. (A) Viability of SKBR-3, N87, NCI–H1975, and PC9 cells incubated with 1 mg/mL purified proteins for 12 and 24 h. (B, C) LDH release (B) and Annexin V/PI flow cytometry analyses of (C) of SKBR-3 cells incubated with 1 mg/mL purified proteins for 24 h. (D) Pyroptotic morphology of SKBR-3 cells treated with the indicated immunopyroptotins for 12 h. Data are expressed as mean ± standard error of the mean. n = 3, *P < 0.05, **P < 0.01, ***P < 0.001, ****P < 0.0001 by *t*-test.

3. Results

3.1. Identification of the purified long-lasting immunopyroptotins

Two long-lasting immunopyroptotins—ABD035-immunoGN and dAb7h8-immunoGN—were constructed based on immunotBid, as previously reported [16]. This was achieved by inserting an albumin-binding peptide of bacterial or human origin between the anti-HER2 scFv P1h3 and the membrane translocation peptides and by replacing the active pyroptotic effector GN with the parental apoptotic tBid (Fig. 1A). ImmunoGN was used as a control to exclude the albumin-binding domains. To facilitate protein purification, immunoGN derivatives were fused to a His-tag at the C-terminus. Furthermore, 293F cells transfected with the abovementioned constructs were harvested after 5 d, and immunopyroptotins expressed in eukaryotic expression systems were purified using Ni^{2+}-NTA affinity chromatography. All the proteins of interest were detected through western blotting using an anti-His antibody (Fig. 1B and S9A). The purified fusion proteins were quantified using BCA assay and by conducting grayscale analysis of the protein electrophoresis gel (Fig. 1C and S9B). The estimated concentrations of ABD035-immunoGN, dAb7h8-immunoGN, immunoGN, and immunotBid were 1 mg/mL, 1.2 mg/mL, 1.4 mg/mL, and 2 mg/mL, respectively.

3.2. Killing capacity of the long-lasting immunopyroptotins in vitro

To explore the tumor-killing capacity of the purified immunopyroptotins, cell viability was assessed in several cancer cell lines, including SKBR-3 and N87 cells with HER2 high expression, NCI–H1975 cells with HER2 medium expression, and HER2-null PC9 cells

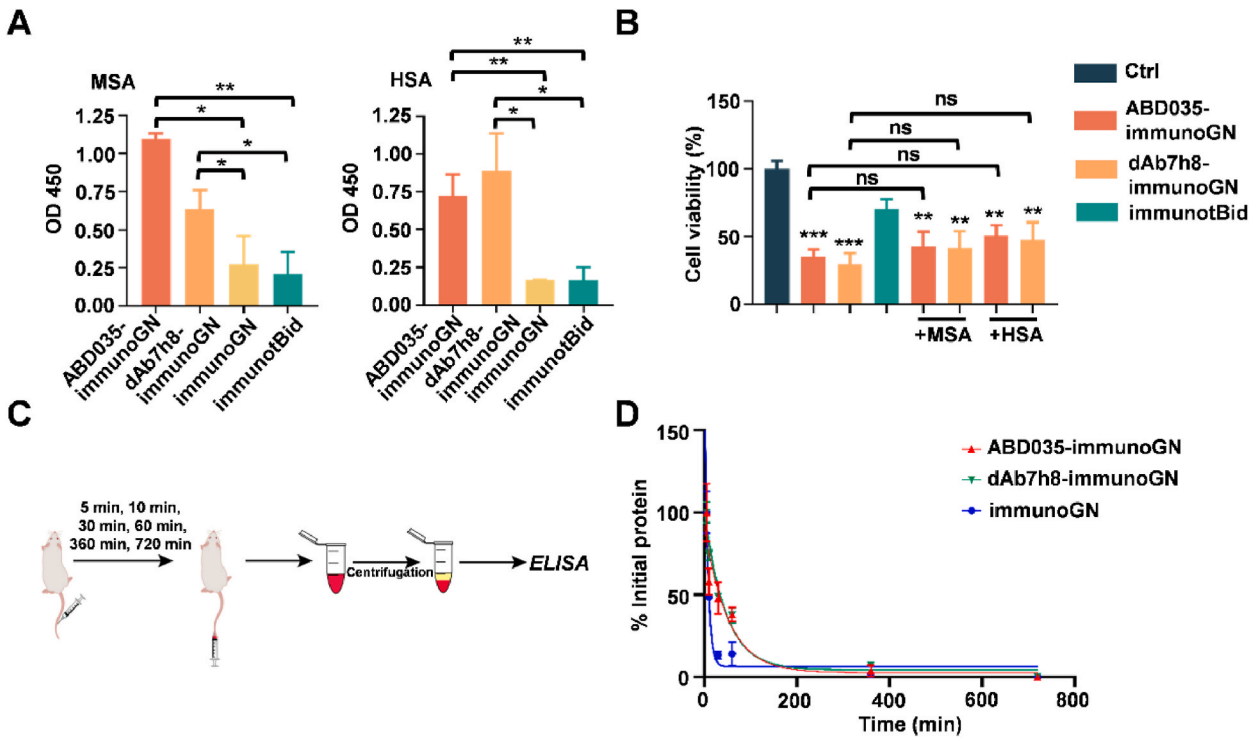

E

Proteins no.	Half, min	AUC	SE
ABD035-immunoGN	35.22	9717	1018
dAb7h8-immunoGN	31.25	10858	721
immunoGN	4.599	4043	1077

Fig. 3. Albumin-binding affinity of the long-lasting immunopyroptotins in vitro and in vivo. (A) In vitro tests of 1 μg/mL MSA- and 1 μg/mL HSA-bound immunopyroptotins measured using ELISA. (B) Viability of SKBR-3 cells incubated with 1 μg/mL MSA- and 1 μg/mL HSA-bound immunopyroptotins for 24 h. (C) Schematics showing measurement of in vivo pharmacokinetics of the immunopyroptotins. BALB/C mice were injected intravenously with 0.1 μmol/kg of proteins. Blood samples were collected at the indicated times. The levels of immunopyroptotins in mouse blood were assessed by ELISA. (D) Pharmacokinetics of ABD035-immunoGN and dAb7h8-immunoGN proteins in mice. n = 3 mice per group. (E) Quantification of (D). Data are expressed as mean ± standard error of the mean. n = 3, *P < 0.05, **P < 0.01, ***P < 0.001 by *t*-test.

[16]. The two long-lasting immunopyroptotins showed selective cytotoxicity toward HER2-positive tumor cells, with undetectable killing of HER2-negative tumor cells (Fig. 2A). ABD035-immunoGN and dAb7h8-immunoGN exerted comparably higher cytotoxic effects on SKBR-3 and N87 cells than those of immunotBid, and this difference in the killing capacity of the immunopyroptotins and immunoapoptotins was further amplified at 24 h post-treatment. These two immunopyroptotins killed relatively fewer NCI–H1975 cells. Data from both the LDH release and Annexin V/ PI assays supported the notion that immunopyroptotins had a more potent killing capacity in SKBR-3 cells than did the immunotBid control (Fig. 2B and C, and S1). GSDMD-N expression in the immunopyroptotin group was higher than that in the control group (Figs. S2 and S10). The dying cells in the immunopyroptotin-treated groups showed pyroptotic morphology with large bubbles appearing on the plasma membrane (Fig. 2D).

3.3. Albumin-binding affinity of the long-lasting immunopyroptotins

To analyze albumin-binding capability, ELISA was performed using an anti-His antibody to detect long-lasting immunopyroptotins bound to 96-well plates coated with HSA and MSA. ABD035-immunoGN and dAb7h8-immunoGN showed robust binding to both HSA and MSA in vitro compared to the non-binding controls, immunoGN, and immunotBid (Fig. 3A).

Next, we used CCK-8 assays to determine whether the MSA- or HSA-binding activities affected the cytotoxicity abilities of immunopyroptotins. There was no significant difference in the killing capacity of either ABD035-immunoGN or dAb7h8-immunoGN, regardless of their binding to MSA or HSA (Fig. 3B).

3.4. Prolonged in vivo half-life of the long-lasting immunopyroptotins

The presence of ABD035-immunoGN and dAb7h8-immunoGN in the serum of nude mice was monitored at 5, 10, 30, 60, 360, and 720 min after intravenous injection of 0.1 μmol/kg of the indicated proteins (Fig. 3C). As expected, the half-life of the albumin-binding domain-deficient immunoGN control group was less than 5 min. In contrast, the serum half-lives of ABD035-immunoGN and dAb7h8-immunoGN were much longer, with a 7-fold increase up to approximately 30 min (Fig. 3D and E). Significant accumulation of long-lasting immunopyroptotins was observed in 4T1-hHER2 transplanted tumors as compared to that of the immunoGN control (Fig. 4A and B).

3.5. Antitumor effect of the long-lasting immunopyroptotins in N87 xenograft nude mice

To evaluate therapeutic efficacy in T cell-deficient mice, nude mice bearing N87 tumors were intravenously administered four doses of 0.1 μmol/kg of the long-lasting immunopyroptotins proteins every other day; immunotBid treatment used employed as a positive control (Fig. 5A). Mice receiving ABD035-immunoGN and dAb7h8-immunoGN demonstrated a stronger suppression of tumor growth than that showed by immunotBid-treated mice (Fig. 5B and C). The retarded tumor growth caused by the long-lasting immunopyroptotins prolonged animal survival (Fig. 5D), and the secretion of inflammatory factors of IL-1β and IL-18 was promoted in tumors (Fig. S3). No systemic toxicity was observed in ABD035-immunoGN- and dAb7h8-immunoGN-treated mice at these therapeutic doses (Fig. S4).

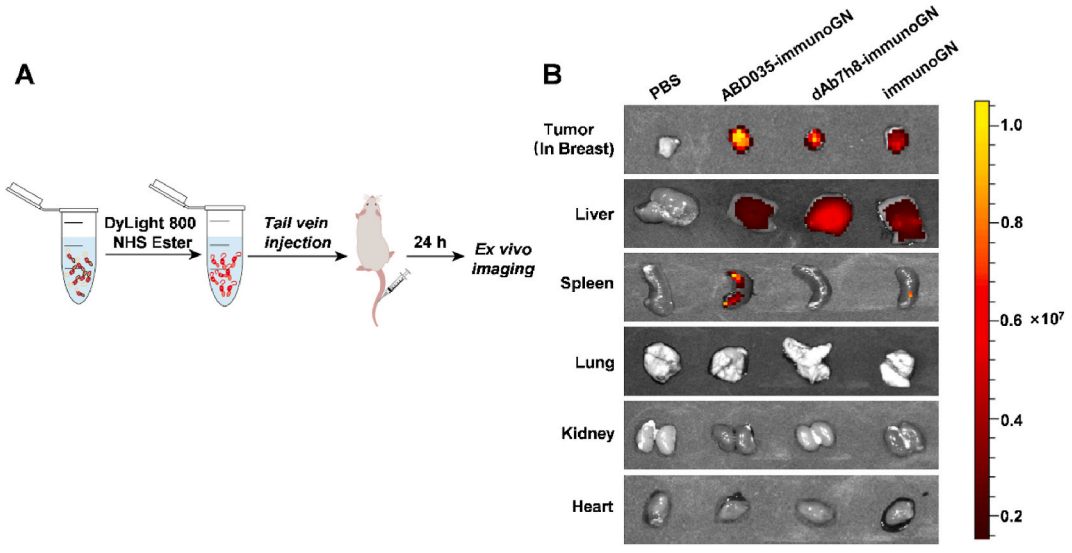

Fig. 4. Targeting efficiency of the long-lasting immunopyroptotins in 4T1-hHER2 tumor-bearing BALB/c mice. (A) Schematics showing measurement of targeting efficiency of the immunopyroptotins. (B) Representative ex vivo images of distribution in tumor and major organs of the immunopyroptotins labeled with DyLight 800 NHS Ester 24 h after tail vein injection. n = 3 mice for each group.

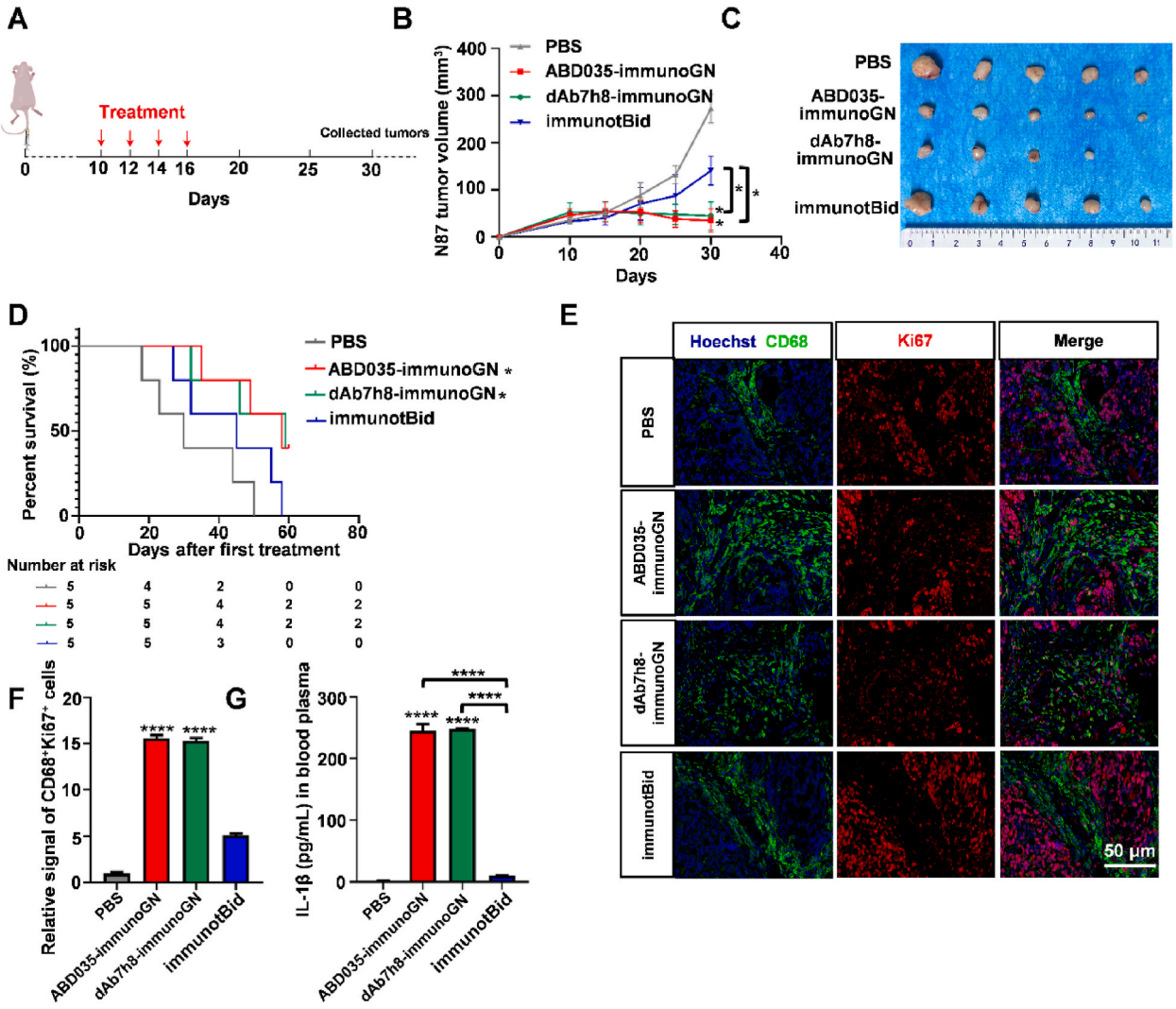

Fig. 5. Therapeutic efficacy of the long-lasting immunopyroptotins in N87 tumor-bearing nude mice. (A) The experimental procedure is illustrated in a schematic. The fusion proteins were intravenously injected four times every 2 d. Tumor volumes were recorded every 5 d until day 30. (B) Examination of mean tumor growth in the mice. n = 5 mice per group. Data are expressed as mean ± SEM. *P < 0.05 by two-way ANOVA. (C) Photographs of representative tumors are shown. n = 5 mice per group. (D) Survival curves of the mice treated with the indicated proteins. n = 5 mice per group. *P < 0.05 by log-rank test. (E) Immunofluorescence staining of $CD68^+$ $Ki67^+$ cells in the tumors after administration of immunopyroptotins. n = 3 mice. (F) Quantification of (E). (G) The secretion of IL-1β in blood plasma. Data are expressed as mean ± SEM, n = 3. *P < 0.05, ****P < 0.0001 by *t*-test.

Next, we assessed whether macrophages contributed to the antitumor effects in treated nude mice. Administration of ABD035-immunoGN and dAb7h8-immunoGN remarkably promoted macrophage proliferation, as evidenced by the increased number of $CD68^+$ $Ki67^+$ cells localized in the tumors (Fig. 5E and F). The secretion of IL-1β in blood plasma also increased in the long-lasting immunopyroptotin groups as compared with that in the control groups (Fig. 5G). These results suggest that immunopyroptotins have enhanced tumor-suppressive functions in T cell-deficient mice, which may involve macrophage-mediated antitumor immune responses.

3.6. Antitumor immune responses of the long-lasting immunopyroptotins in bilateral breast tumor-bearing BALB/c mice

Immunocompetent mice were used to investigate the antitumor immune responses to ABD035-immunoGN. We constructed a breast tumor BALB/c mouse model bearing 4T1-hHER2 tumors bilaterally and intratumorally injected four doses of ABD035-immunoGN into one side to determine whether the corresponding untreated tumor could be repressed (Fig. 6A). Notably, ABD035-immunoGN potently inhibited tumor growth in both injected and distant tumors (Fig. 6B and C), leading to an increased survival rate in mice (Fig. 6D) and inhibition of lung metastasis (Fig. S5).

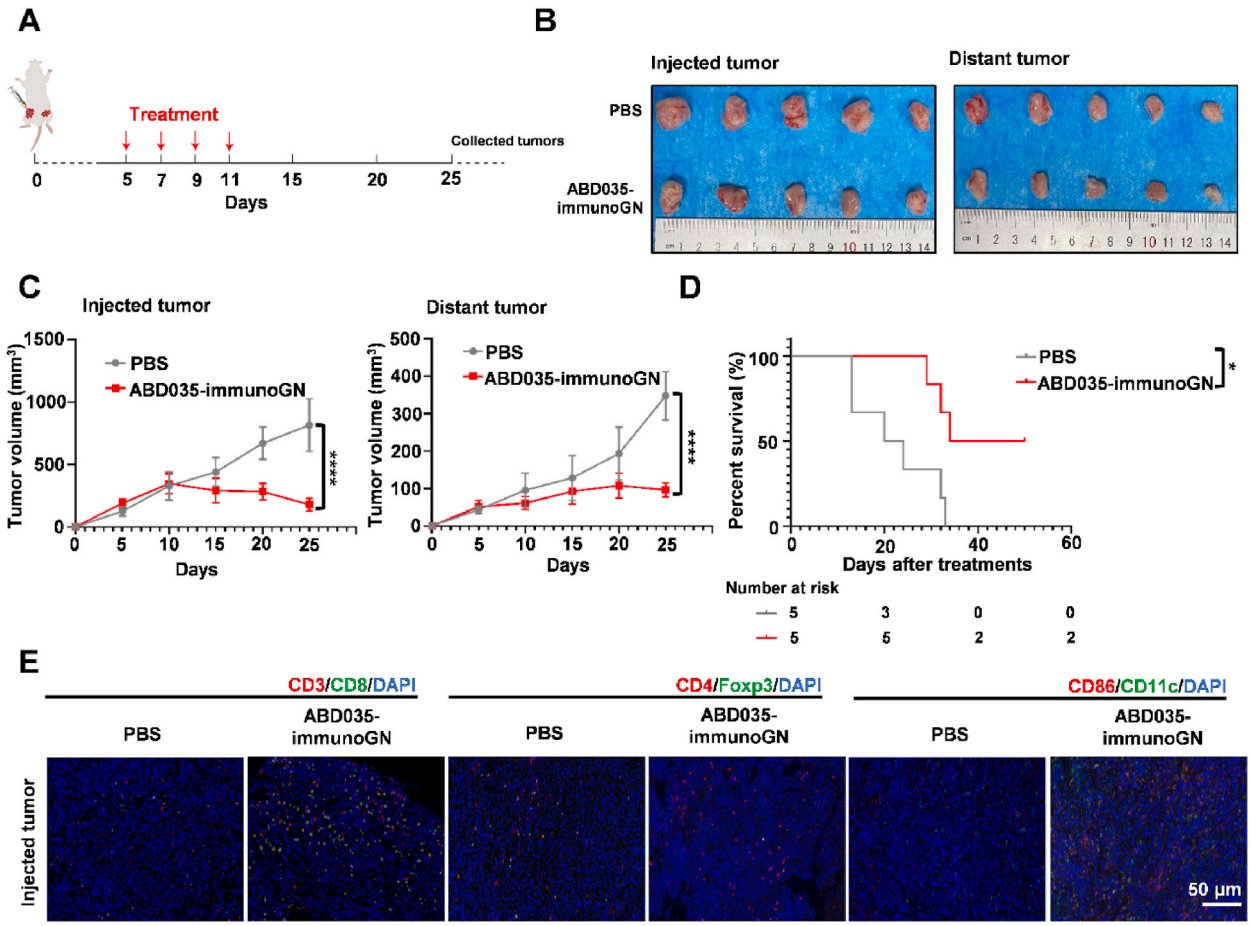

Fig. 6. Enhanced antitumor immune responses of the long-lasting immunopyroptotins in 4T1-hHER2 bilateral tumor-bearing BALB/c mice. (A) Schematic diagram of the experiment. The fusion proteins were administered intratumorally on the left side every other day. Tumor volumes were measured and recorded every 5 d until day 25. (B) Representative photographs of tumors are shown. n = 5 mice per group. (C) Tumor volume growth curves. n = 5 mice per group. Data are expressed as mean ± SEM. ****P < 0.0001 by two-way ANOVA. (D) Survival curves of the recipient mice. n = 5 mice per group. *P < 0.05 by log-rank. (E) Immunofluorescence staining of $CD3^+$ $CD8^+$ T cells, $CD4^+$ $Foxp3^+$ T cells, and $CD86^+$ $CD11C^+$ DC in the injected tumors. n = 3 mice.

To better understand the mechanism underlying the observed systemic antitumor effects, injected tumors and lymph nodes were subjected to immunofluorescence and/or flow cytometry to detect immune cell signatures. Compared to that in the PBS group, the accumulation of antitumor $CD3^+$ $CD8^+$ T cells and mature DCs (Fig. 6E–S6 and 7A-7F) was enhanced in the ABD035-immunoGN-treated tumors and lymph nodes. In contrast, decreased numbers of $CD4^+$ $Foxp3^+$ Tregs were observed in the injected tumors of mice receiving ABD035-immunoGN treatment compared to those in the control (Fig. 6E). The expression of inflammatory cytokines was analyzed in injected tumors. Tumors treated with ABD035-immunoGN exhibited upregulated expression of the proinflammatory cytokines IL-2 and IFN-γ (Fig. 7G) and downregulated expression of the anti-inflammatory cytokines IL-10 and TGF-β, as well as the immunosuppressive Foxp3 marker (Fig. 7H). The secretion of inflammatory factors of IL-1β, IL-18, and HMGB1 in blood plasma and the injected tumors also increased in the long-lasting immunopyroptotin-recipient mice as compared with that in the control group (Fig. S7).

To further investigate antitumor immunity in mice with ABD035-immunoGN-non-injected distant tumors, we assessed tumor-infiltrating immune cells from distant tumors using flow cytometry and immunofluorescence analyses. Contralateral treatment with ABD035-immunoGN increased the number of $CD3^+$ $CD8^+$ T cells in distant tumors (Figures S6, 8A-8C and 8E). In contrast, the number of $CD4^+$ $Foxp3^+$ T cells decreased in distant tumors after treatment with ABD035-immunoGN (Fig. 8D and E). Therapeutic doses of ABD035-immunoGN caused no detectable morphological abnormalities in the major organs of the 4T1-hHER2 tumor-bearing BALB/c mice (Figs. S7A and S7B). Despite the unaltered serum levels of ALT and AST, the ABD035-immunoGN-treated mice showed a slight increase in CREA levels, indicating mild renal function damage (Fig. S8D). Taken together, these results demonstrated that ABD035-immunoGN strongly elicited systemic antitumor immune responses via increased infiltration of $CD3^+$ $CD8^+$ T cells and mature DCs, leading to effective regression of tumors outside the injection sites.

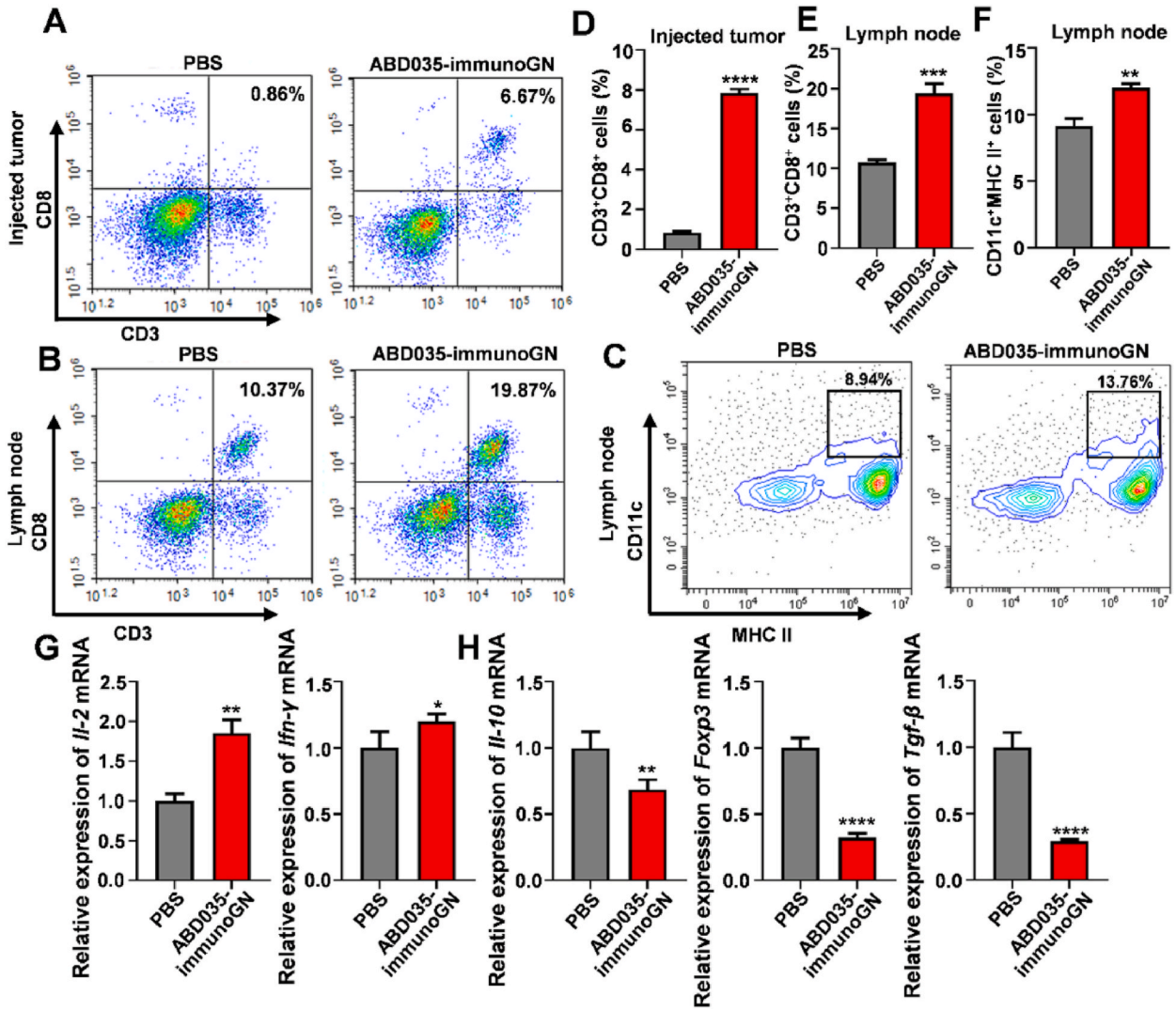

Fig. 7. Long-lasting immunopyroptotins boost antitumor immunity in 4T1-hHER2 bilateral tumor-bearing BALB/c mice. (A, B) Flow cytometric quantification of $CD3^+$ $CD8^+$ T cells infiltrated in the injected tumors (A) and lymph nodes (B). n = 3 mice. (C) Flow cytometric quantification of $CD11c^+$ $MHCII^+$ cells infiltrated in the lymph nodes. n = 3 mice. (D–F) Quantification of (A–C). n = 3, **P < 0.01, ***P < 0.001, ****P < 0.0001 by *t*-test. (G, H) Relative gene expression of proinflammatory cytokines (G), anti-inflammatory cytokines and immunosuppressive Foxp3 marker (H) in the injected tumors. n = 3 mice, *P < 0.05, **P < 0.01, ****P < 0.0001 by *t*-test.

4. Discussion

Pyroptosis, a type of programmed cell death, is characterized by the formation of pores in cell membranes via proteins of the GSDM family, causing cell swelling and cytomembrane ruptures, as well as the release of proinflammatory cytokines IL-1β and IL-18, triggering a strong inflammatory response [34,35]. GSDM-induced pyroptosis is thought to exert a kinetic advantage over either caspase- or tBid-induced apoptosis because these apoptotic effectors indirectly trigger a multistep cell death process by sequentially interacting with other downstream molecules. In contrast, the pyroptotic effector GSDM directly induces single-step cell death via its pore-forming capability.

The feasibility of using a pyroptosis-inducing strategy in cultured cells has been previously demonstrated. Transfecting the N-terminal gene fragments of GSDMA, GSDMC, or GSDME induces significant pyroptosis in human 293T cells, unlike the transfectants with their full-length gene counterparts, which lack killing effects [19]. Thus, the overexpression of the GSDM-N domain can kill mammalian cells via intrinsic cytotoxicity. Addition of either the purified active form of a non-covalently linked complex of full-length GSDMD or the truncated GSDMA-N terminal domain to the culture media of murine bone marrow-derived macrophages did not induce successful cell lysis. Conversely, cytosolic delivery of the purified GSDM-N terminal domain resulted in cytotoxicity, suggesting that access to the inner cell membranes is required for pore formation [19]. Similar results have been observed in human 293T cells [19].

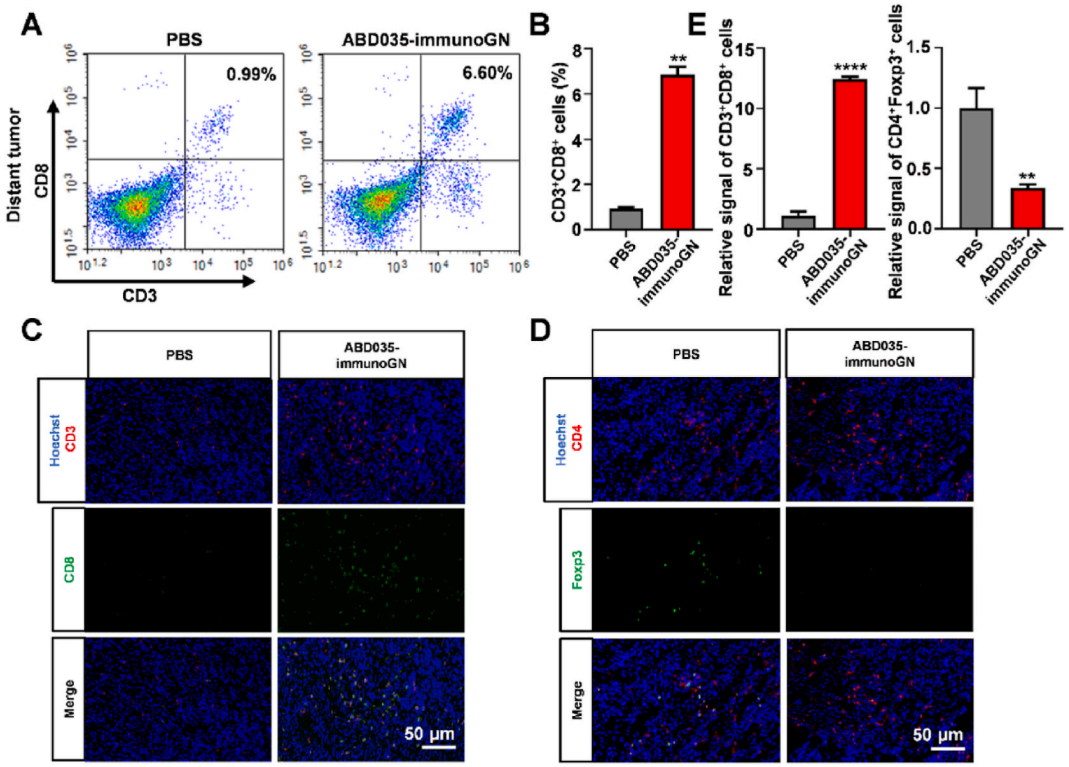

Fig. 8. Long-lasting immunopyroptotins promote cytotoxic T cell infiltration in distant tumors of 4T1-hHER2 bilateral tumor-bearing BALB/c mice. (A) Flow cytometric quantification of $CD3^+$ $CD8^+$ T cells infiltrated in the distant tumors. n = 3 mice. (B) Quantification of (A). n = 5, **P < 0.01 by *t*-test. (C) Representative immunofluorescence staining of $CD3^+$ $CD8^+$ T cells in the distant tumors. (D) Representative immunofluorescence staining of $CD4^+$ $Foxp3^+$ T cells in the distant tumors. n = 3 mice. (E) Quantification of (C, D). n = 5, **P < 0.01, ****P < 0.0001 by *t*-test.

Taken together, the cellular introduction of N-terminal GSDM fragments induces pyroptosis only when delivered cytosolically but not extracellularly.

Extended application of pyroptosis-based antitumor strategies requires pyroptotic induction, specifically in tumor cells. Recent studies have focused on two major types of nanotechnological design. One such design is the elegantly controlled regulation of the intratumoral activation of endogenous GSDM proteins. For example, photosensitizer-encapsulated nanoparticles are endocytosed into tumor cells to release loaded photosensitizers via either an acid-activated mechanism [36] or homing of wrapped tumor membranes [37]. Subsequently, they underwent photoactivation for endogenous caspase-3/GSDME cleavage, followed by cytomembrane perforation. Photoactivated tumor cell pyroptosis can be facilitated by co-loading epigenetic regulators such as decitabine in photosensitizer-carrying nanovesicles to upregulate GSDME expression in tumor cells [37]. Another example is the reconstitution of the attenuated bacterium Listeria monocytogenes coated with red blood cell membranes, which results in the upregulation of endogenous GSDMC expression and activation of the caspase-8/GSDMC axis for tumor cell pyroptosis [38]. Another design harnesses cancer-imaging probe-cleaved release from the nanoparticles of a modified full-length GSDMA3 with the loss of the inhibitory function of its C-terminal domain [34]. As shown in these reports, antitumor immune responses are elevated, which can be attributed to robust pyroptosis in tumors.

This study tested an alternative antitumor pyroptotic strategy using nanotechnology-independent delivery of a constitutively active N-terminus of GSDMD, specifically into tumor cells. We generated and purified a class of HER2-targeted immunopyroptotins using the formula P1h3-ABD035(dAb7h8)-B2-E5C3-GSDMD-N. This design offers two benefits. First, immunopyroptotins would deliver active GSDMD-N directly into the cytosol of HER2-positive tumor cells, effectively inducing pyroptosis and selectively targeting tumor cells while sparing normal cells. Second, immunopyroptotins would bind to albumins, potentially extending their serum half-life.

Enhanced tumor killing both in vitro and in vivo was demonstrated by immunopyroptotins, with ImmunotBid used as a control. The two types of immunopyroptotins exhibited comparable killing capacities in vitro. ABD035-immunoGN showed a 41 % increase in killing rates against SKBR-3 cells compared to those of immunotBid at 24 h post-treatment. Similarly, the cytotoxicity of ABD035-immunoGN in N87 cells reached as high as 62 %, compared to 38 % for immunotBid after 24 h of incubation. The immunopyroptotin-augmented in vivo anti-tumor effect was further confirmed in T cell-deficient and immunocompetent tumor mouse models. In N87 tumor nude mice, ABD035-immunoGN-caused tumor regression was 38 % stronger than that of immunotBid-induced tumor inhibition, with 35 % stronger tumor suppression in dAb7h8-immunoGN than in immunotBid. In BALB/c mice with 4T1-hHER2

bilateral tumors, ABD035-immunoGN-injected tumors demonstrated 78 % suppression, accompanied by 72 % growth inhibition of non-injected distant tumors.

The prolongation of the lifetime of immunopyroptotins was confirmed in nude mice. Although the eukaryotically purified immunopyroptotins were not highly pure, there was a 7-fold increase in the serum half-life of long-lasting immunopyroptotins compared to that of their counterparts without the albumin-binding domain. This improvement is comparable to that reported by Wei et al., in which immunotoxins were reconstituted with an albumin-binding domain from *Streptococcus*, showing a 10-fold increase in half-life over the original albumin-binding domain-null counterpart [24].

Next, we investigated whether antitumor immunity was potentiated primarily in immunocompetent mice treated with immunopyroptotins. In immunocompetent BALB/c mice bilaterally bearing 4T1-hHER2 tumors, intratumoral $CD3^+$ $CD8^+$ T cells and $CD86^+$ $CD11c^+$ mature DCs accumulated to a greater extent in the immunopyroptotin-injected tumors than in the tumors of the control group. Immunopyroptotins also exerted a growth-suppressive effect on non-injected distant tumors, with increased intratumoral infiltration of cytotoxic T cells. These findings indicated that tumor-specific pyroptosis induction can activate systemic antitumor immune responses. However, persistent high levels of antigen released by dying pyroptotic tumor cells may drive functional exhaustion of T cells. Further research is necessary to clarify the potential immune suppressive function and the mechanism of immune responses of immunopyroptotins in cancer therapies. It was also noted that in T cell-null nude mice bearing N87 tumors, macrophage infiltration increased in the tumor tissues of the ABD035-immunoGN and dAb7h8-immunoGN groups compared to that in the tumor tissues of the immunotBid control group. Yet it remains to be further investigated whether the increase of macrophage infiltration in these immunodeficient mice would have an additive effect on antitumor function of immunopyroptotins.

However, some concerns including the feasibility and challenges of translating these immunopyroptotins into clinical applications remain to be addressed [39]. First, the eukaryotic purification method optimized herein failed to produce immunopyroptotic proteins in large quantities with high purity. Further efforts should be made to optimize high-yield expression and purification systems for secretory immunopyroptotins. Second, the half-life of albumin-bound immunopyroptotins, although seven times longer than that of the albumin-binding domain-deficient control, was still as short as 30 min. Further optimization of the structural design of immunopyroptotins should be considered to overcome this problem. Third, off-tumor toxicity by HER2-targeted therapeutics poses a potential risk, given low-level expression of HER2 in some of normal tissues. But in this study, nonspecific toxicity was not observed at therapeutic doses, as supported by the absence of both morphological abnormalities in the major organs and biochemical abnormalities in serum of the immunopyroptotin-recipient mice (Figs. S8A–S8C). More importantly, as we previously reported, anti-HER2 antibody-caspase conjugates are capable of killing trastuzumab-resistant cancer cells [40]. Thus this antibody-guided pyroptotic induction strategy would provide a promising alternative for HER2-targeted therapeutics especially in the case of trastuzumab resistance [41], and further investigation is needed concerning whether the immunopyroptotins could exert additive or synergistic effects with trastuzumab or other HER2-targeted drugs [42]. Lastly, patients suitable for the immunopyroptotin treatment should be carefully selected by the more efficient HER2 diagnostic methods [43,44], and therapeutic efficacy should also be evaluated in patients with different levels of HER2 expression.

5. Conclusion

We constructed and purified long-lasting immunopyroptotins against HER2 using eukaryotic methods. These fusion proteins exhibited potent tumor growth-inhibitory effects and induced systemic antitumor immune responses in both T cell-deficient N87 tumors and immunocompetent 4T1-hHER2 tumor mouse models. This study presents a new strategy for the direct application of a constitutively active GSDM N-terminal peptide in combination with a tumor-targeting antibody for pyroptosis-based tumor therapy.

Funding

This work was supported by the National Natural Science Foundation of China under Grant 81972871 and 82373171 (to J.Z).

Data availability statement

The data supporting the findings of this study are available from the corresponding author upon reasonable request.

Ethics approval and consent to participate

The goal of the current study was to inhibit tumor growth using long-lasting immunopyroptotins against HER2. The most efficient and necessary method in this study to confirm the therapeutic effect of the fusion proteins on the tumor growth-inhibitory effect and systemic antitumor immune responses was animal model validation. In our study, 6–8 week female nude mice (n = 40) and 6–8 week female BALB/c mice (n = 53) were supplied by the Fourth Military Medical University (Xi' an, China) and carefully housed in the Laboratory Animal Center. Three to five mice were housed in each cage under pathogen-free conditions with a 12/12-h light/dark cycle and *ad libitum* access to food and water. All mice were anesthetized with isoflurane and used for the in vivo experiments. All the experimental procedures were approved by the Animal Experimental Ethics Committee of the Fourth Military Medical University (approval number: Ref. No. IACUC-20200655). At the end of the study, all the mice were euthanized. All animal experiments were performed according to the ARRIVE guidelines.

CRediT authorship contribution statement

Yuqi Xing: Writing – original draft, Methodology, Investigation, Formal analysis, Data curation. **Feiyu Zhang:** Methodology, Investigation, Formal analysis, Conceptualization. **Tian Yang:** Methodology, Investigation, Conceptualization. **Chunhui Yin:** Investigation, Formal analysis. **Angang Yang:** Visualization, Validation, Supervision, Project administration, Funding acquisition. **Bo Yan:** Visualization, Project administration, Methodology, Investigation. **Jing Zhao:** Writing – review & editing, Writing – original draft, Visualization, Validation, Supervision, Project administration, Methodology, Funding acquisition, Conceptualization.

Declaration of competing interest

The authors declare the following financial interests/personal relationships which may be considered as potential competing interests: Jing Zhao reports financial support was provided by National Natural Science Foundation of China. If there are other authors, they declare that they have no known competing financial interests or personal relationships that could have appeared to influence the work reported in this paper.

Acknowledgments

We are very grateful to the technical help of Yongzhan Nie and Sheng Zhao from the State Laboratory of Cancer Biology, Department of Gastrointestinal Surgery, Xijing Hospital of Digestive Diseases, Fourth Military Medical University, and Mao Sun from the State Laboratory of Cancer Biology, Department of Biochemistry and Molecular Biology, Fourth Military Medical University.

Appendix A. Supplementary data

Supplementary data to this article can be found online at https://doi.org/10.1016/j.heliyon.2024.e30444.

References

[1] M.F. Rimawi, R. Schiff, C.K. Osborne, Targeting HER2 for the treatment of breast cancer, Annu. Rev. Med. 66 (2015) 111–128.
[2] E. Cruz, V. Kayser, Monoclonal antibody therapy of solid tumors: clinical limitations and novel strategies to enhance treatment efficacy, Biologics 13 (2019) 33–51.
[3] L.J. Brown, et al., Heart failure therapies for the prevention of HER2-monoclonal antibody-mediated cardiotoxicity: a systematic review and meta-analysis of randomized trials, Cancers 13 (21) (2021).
[4] S. Yu, et al., Development and clinical application of anti-HER2 monoclonal and bispecific antibodies for cancer treatment, Exp. Hematol. Oncol. 6 (2017) 31.
[5] M.E. Tesch, K.A. Gelmon, Targeting HER2 in breast cancer: latest developments on treatment sequencing and the introduction of biosimilars, Drugs 80 (17) (2020) 1811–1830.
[6] D.J. Wong, S.A. Hurvitz, Recent advances in the development of anti-HER2 antibodies and antibody-drug conjugates, Ann. Transl. Med. 2 (12) (2014) 122.
[7] M.W. Pedersen, et al., Targeting three distinct HER2 domains with a recombinant antibody mixture overcomes trastuzumab resistance, Mol. Cancer Therapeut. 14 (3) (2015) 669–680.
[8] S. Verma, et al., Trastuzumab emtansine for HER2-positive advanced breast cancer, N. Engl. J. Med. 367 (19) (2012) 1783–1791.
[9] S. Modi, et al., Trastuzumab deruxtecan in previously treated HER2-positive breast cancer, N. Engl. J. Med. 382 (7) (2020) 610–621.
[10] M.A. Lyu, R. Kurzrock, M.G. Rosenblum, The immunocytokine scFv23/TNF targeting HER-2/neu induces synergistic cytotoxic effects with 5-fluorouracil in TNF-resistant pancreatic cancer cell lines, Biochem. Pharmacol. 75 (4) (2008) 836–846.
[11] L.T. Jia, et al., Specific tumoricidal activity of a secreted proapoptotic protein consisting of HER2 antibody and constitutively active caspase-3, Cancer Res. 63 (12) (2003) 3257–3262.
[12] J. Zhao, et al., Secreted antibody/granzyme B fusion protein stimulates selective killing of HER2-overexpressing tumor cells, J. Biol. Chem. 279 (20) (2004) 21343–21348.
[13] X.C. Qiu, et al., Single-chain antibody/activated BID chimeric protein effectively suppresses HER2-positive tumor growth, Mol. Cancer Therapeut. 7 (7) (2008) 1890–1899.
[14] T. Wang, et al., Recombinant immunoproapoptotic proteins with furin site can translocate and kill HER2-positive cancer cells, Cancer Res. 67 (24) (2007) 11830–11839.
[15] F. Wang, et al., Selective cytotoxicity to HER2-positive tumor cells by a recombinant e23sFv-TD-tBID protein containing a furin cleavage sequence, Clin. Cancer Res. 16 (8) (2010) 2284–2294.
[16] Q. Ou-Yang, et al., Construction of humanized anti-HER2 single-chain variable fragments (husFvs) and achievement of potent tumor suppression with the reconstituted husFv-Fdt-tBid immunoapoptotin, Biomaterials 178 (2018) 170–182.
[17] J. Shi, W. Gao, F. Shao, Pyroptosis: gasdermin-mediated programmed necrotic cell death, Trends Biochem. Sci. 42 (4) (2017) 245–254.
[18] J. Shi, et al., Cleavage of GSDMD by inflammatory caspases determines pyroptotic cell death, Nature 526 (7575) (2015) 660–665.
[19] J. Ding, et al., Pore-forming activity and structural autoinhibition of the gasdermin family, Nature 535 (7610) (2016) 111–116.
[20] J. Shi, et al., Inflammatory caspases are innate immune receptors for intracellular LPS, Nature 514 (7521) (2014) 187–192.
[21] N. Kayagaki, et al., Caspase-11 cleaves gasdermin D for non-canonical inflammasome signalling, Nature 526 (7575) (2015) 666–671.
[22] Y. Zhang, T. Sun, C. Jiang, Biomacromolecules as carriers in drug delivery and tissue engineering, Acta Pharm. Sin. B 8 (1) (2018) 34–50.
[23] R. Li, et al., Fusion to an albumin-binding domain with a high affinity for albumin extends the circulatory half-life and enhances the in vivo antitumor effects of human TRAIL, J. Contr. Release 228 (2016) 96–106.
[24] J. Wei, et al., Recombinant immunotoxins with albumin-binding domains have long half-lives and high antitumor activity, Proc. Natl. Acad. Sci. U. S. A. 115 (15) (2018) E3501–E3508.
[25] R. Guo, et al., Fusion of an albumin-binding domain extends the half-life of immunotoxins, Int. J. Pharm. 511 (1) (2016) 538–549.
[26] L.J. Holt, et al., Anti-serum albumin domain antibodies for extending the half-lives of short lived drugs, Protein Eng. Des. Sel. 21 (5) (2008) 283–288.
[27] A. Walker, et al., Anti-serum albumin domain antibodies in the development of highly potent, efficacious and long-acting interferon, Protein Eng. Des. Sel. 23 (4) (2010) 271–278.

[28] R.L. O'Connor-Semmes, et al., GSK2374697, a novel albumin-binding domain antibody (AlbudAb), extends systemic exposure of exendin-4: first study in humans–PK/PD and safety, Clin. Pharmacol. Ther. 96 (6) (2014) 704–712.
[29] M.K. Shim, et al., Cancer-specific drug-drug nanoparticles of pro-apoptotic and cathepsin B-cleavable peptide-conjugated doxorubicin for drug-resistant cancer therapy, Biomaterials 261 (2020) 120347.
[30] M.K. Shim, et al., Carrier-free nanoparticles of cathepsin B-cleavable peptide-conjugated doxorubicin prodrug for cancer targeting therapy, J. Contr. Release 294 (2019) 376–389.
[31] G.L. DeNardo, S.J. DeNardo, Evaluation of a cathepsin-cleavable peptide linked radioimmunoconjugate of a panadenocarcinoma MAb, m170, in mice and patients, Cancer Biother. Radiopharm. 19 (1) (2004) 85–92.
[32] J. Chang, et al., [Application of molecular chaperones to soluble expression of e23sFv/His fusion proteins], Xi Bao Yu Fen Zi Mian Yi Xue Za Zhi 31 (9) (2015) 1205–1210.
[33] K.J. Livak, T.D. Schmittgen, Analysis of relative gene expression data using real-time quantitative PCR and the 2(-Delta Delta C(T)) Method, Methods 25 (4) (2001) 402–408.
[34] Q. Wang, et al., A bioorthogonal system reveals antitumour immune function of pyroptosis, Nature 579 (7799) (2020) 421–426.
[35] R. Loveless, R. Bloomquist, Y. Teng, Pyroptosis at the forefront of anticancer immunity, J. Exp. Clin. Cancer Res. 40 (1) (2021) 264.
[36] B. Chen, et al., A pyroptosis nanotuner for cancer therapy, Nat. Nanotechnol 17 (7) (2022) 788–798.
[37] P. Zhao, et al., Programming cell pyroptosis with biomimetic nanoparticles for solid tumor immunotherapy, Biomaterials 254 (2020) 120142.
[38] Y. Liu, et al., Intravenous delivery of living Listeria monocytogenes elicits gasdmermin-dependent tumor pyroptosis and motivates anti-tumor immune response, ACS Nano 16 (3) (2022) 4102–4115.
[39] F. Schettini, F. Giudici, D. Generali, Therapeutic resistance and optimal drug sequencing in HER2-positive metastatic breast cancer: unmet needs and future perspectives, Heliyon 10 (1) (2024) e23367.
[40] J.L. Ren, et al., The effect of direct translocation across endosomes on the cytotoxicity of the recombinant protein e23sFv-Fdt-casp6 to HER2 positive gastric cancer cells, Biomaterials 32 (30) (2011) 7641–7650.
[41] R. Du, et al., PDPN positive CAFs contribute to HER2 positive breast cancer resistance to trastuzumab by inhibiting antibody-dependent NK cell-mediated cytotoxicity, Drug Resist. Updates 68 (2023) 100947.
[42] Y. Zou, et al., N6-methyladenosine regulated FGFR4 attenuates ferroptotic cell death in recalcitrant HER2-positive breast cancer, Nat. Commun. 13 (1) (2022) 2672.
[43] S. Klein-Scory, et al., Liquid biopsy based HER2 amplification status in gastric cancer patients indicates clinical response, Heliyon 9 (11) (2023) e21339.
[44] R. Zeng, et al., Smartphone-based photoelectrochemical immunoassay with Co(9)S(8)@ZnIn(2)S(4) for point-of-care diagnosis of breast cancer biomarker, Research 2022 (2022) 9831521.